Field experiment on a scaled prototype of a floating multi-purpose offshore platform: Dynamic response determination with uncertainty quantification

Publisher copyright

(Article begins on next page)

27 February 2025

Field experiment on a scaled prototype of a floating multi-purpose offshore platform: Dynamic response determination with uncertainty quantification

Carlo Ruzzo [a], Giovanni Malara [a], Maurizio Collu [b], Anita Santoro [c], Vincenzo Fiamma [a], Andrea Scialò [a], Fabrizio Lagasco [d], Felice Arena [a], *

[a] *Natural Ocean Engineering Laboratory (NOEL), Mediterranea University, Reggio Calabria, Italy*
[b] *Department of Naval Architecture, Ocean and Marine Engineering, University of Strathclyde, Glasgow, UK*
[c] *Wavenergy.it srl, Reggio Calabria, Italy*
[d] *RINA Consulting S.p.A., Genova, Italy*

ABSTRACT

This paper presents the results of a field experimental campaign on a 1:15 scaled prototype of an innovative floating multi-purpose platform, developed within "The Blue Growth Farm" (BGF) EU H2020 project. The critical technical innovation of the concept is the integration of an industrial aquaculture production system, installed in deep waters, with wind and wave energy harvesting technologies. The article describes the overall structure dynamics based on the analysis of a wide experimental dataset (comprising 5974 records), collected between May and July 2021 at the Natural Ocean Engineering Laboratory (NOEL) of Reggio Calabria (Italy). Specifically, (linearized) response amplitude operators (RAOs) associated with variable environmental conditions are chosen as response indicators, and a comprehensive parametric analysis has been carried out, to assess the optimal criteria for their estimation from the experimental data. The results allowed the identification of the key dynamic properties of the platform concept, including nonlinear effects involved in the overall system dynamics. Furthermore, the novel framework developed here can also be utilized for the analysis and interpretation of other field experimental campaigns on floating offshore structure models.

1. Introduction

The sustainable use of the sea is widely recognized as an important challenge for the next decades (Jouffray et al., 2020), in particular to tackle some big challenges such as the need for sustainable energy and food. Nowadays, the so-called "Blue Growth" is already a reality, as demonstrated by the substantial and increasing number of offshore installations, e.g. in the wind energy industry (Lee et al., 2021). Scientific and commercial interests in this field cover many applications (European Commission and Directorate-General for Maritime Affairs and Fisheries, 2019), where seafood and marine energy represent some of the most important resources envisaged for future exploitation (Clarke and Bostock, 2017; Melikoglu, 2018). For this purpose, development of new platform concepts, fulfilling the requirements of reliability, cost-effectiveness, and sustainability, is pivotal. Since fixed structures tend to become prohibitively expensive as water depth increases, floating platforms are required. In this context, the possibility of integrating multi-purpose functionalities in a single platform has been pro-

posed and investigated, to improve the overall cost-efficiency of the system. Notable examples are H2Ocean, Mermaid and Tropos projects (see Nassar et al. (2020) for a general overview). The development of such concepts is quite complex and requires a multi-disciplinary approach, involving political, economic, social, technological, legal, and environmental (PESTLE) aspects. From a technical point of view, challenges include the description of the coupled dynamics of the novel concepts accounting for the mutual interactions between sub-systems and technologies. Indeed, the latter are described by models that, frequently, involve nonlinear aspects to be resolved (Abhinav et al., 2020). In this context, the experimental testing on scaled models plays an essential role for understanding the physics of these interactions and for the validation of the numerical models utilized for their prediction. However, traditional indoor tests in wave tanks or ocean basins are generally limited in time and impose constraints on the scaling factors, based on the available space and equipment. Such constraints may have an impact on the accuracy with which physical phenomena not scalable by Froude similarity are represented, such as viscous forces on relatively slender

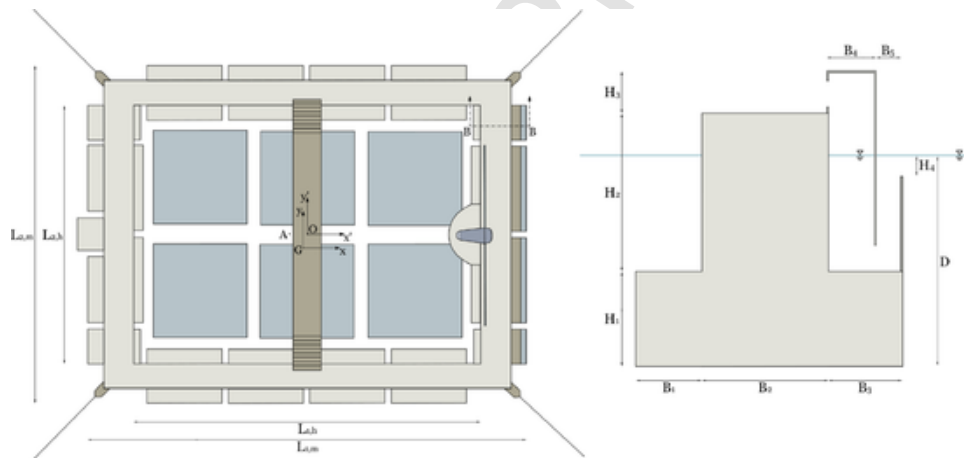**Fig. 1.** - Prototype model object of the test.

Fig. 2. - Schematic representation of the platform: plan view (left panel) and BB section, i.e., frontal section with WEC (right panel).

structural elements (Sarpkaya and Isaacson, 1981), wind (Wen et al., 2020) and wave (Orphin et al., 2022) energy conversion systems. This issue is particularly relevant for multi-purpose floating structures (Ruzzo et al., 2021), characterized by the integration of multiple subsystems, each with its own physical laws. Complementary to indoor activities are intermediate-scale experimental campaigns at sea (Ruzzo et al., 2018). They are generally more expensive in terms of absolute costs, but allow to test the concept in relevant environment, and therefore to achieve a higher Technology Readiness Level (TRL), to develop larger databases of experimental data, thanks to the longer time duration of the tests, and to improve the scaling accuracy. Indeed, larger models suffer less from scale effects and facilitate the application of performance scaling approach for the representation of the above-mentioned non scalable phenomena (Fontanella et al., 2019; Ruzzo et al., 2021; Wen et al., 2020). On the other hand, the interpretation of the measured data is more challenging, mainly due to the fact that the environmental conditions cannot be controlled like in an indoor facility, and due to the non-repeatability of the tests. These facts emphasize the importance of utilizing reliable identification techniques, applicable for concept characterization and numerical model validation.

In this context, the "Blue Growth Farm" project (Lagasco et al., 2019) was aimed at developing an efficient, cost-competitive, and environmentally friendly multi-purpose floating offshore farm platform concept. In particular, it proposed a moored modular floating structure, integrating automated aquaculture, wind turbine, and wave energy

converter (WEC) technologies (Lagasco et al., 2019). The project involved two experimental activities on scale models of the floating platform concept (Ruzzo et al., 2020), which demonstrated its technical feasibility and shed light on its complex coupled dynamic behavior. The first experimental campaign was carried out in October 2019, testing a 1:40 scale model at the Hydrodynamics and Ocean Engineering Tank (HOET) of École Centrale de Nantes (France). In the second experimental campaign, instead, a 1:15 outdoor prototype was tested at the Natural Ocean Engineering Laboratory (NOEL) field site in Reggio Calabria (Italy), between March 2021 and January 2022.

Various configurations of the outdoor prototype model were tested, with the final objective of characterizing the mutual influence of the technologies integrated onboard. Thus, the platform was tested with and without WECs, with the wind turbine operating and not operating (parked conditions), and with and without the fish cages. This article focuses on the configuration where WECs and cages are not present. This configuration is a baseline for the validation of numerical models and constitutes the first step of a series of future analyses, including also wind turbine, WECs and cages dynamic effects. More specifically, the present work focuses on the analysis of the vertical velocity in a point and the roll-pitch motions. The dynamic response is investigated through response amplitude operators (RAOs) estimated from adequately selected sets of input data. Despite the wide use of RAOs to interpret floating structure dynamics in ocean engineering, few studies are available regarding their estimation from irregular wave data. This

Fig. 3. - Wave measuring stations equipped with ultrasonic probes (a), and aluminum pole supporting the AHRS inertial platform (b).
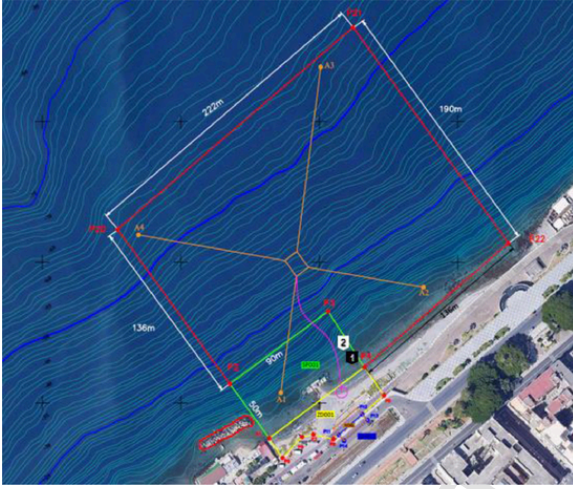
Fig. 4. – Bathymetric map (orthophoto) of the installation site including platform position at equilibrium (orange rectangle), wave stations (indicated by 1, and 2, respectively), and anchors position (A1 ÷ A4).

Table 2
Theoretical undamped natural frequencies of the 1:15 scaled prototype.

DOF	Surge	Sway	Heave-pitch	Roll	Pitch-heave	Yaw
Natural frequency [rad/s]	0.11	0.08	1.52	1.58	1.38	0.20

grees of freedom (6-DOF) are measured by one of the AHRS inertial platforms installed onboard, located on a rigid aluminum pole bolted to the structure hull (Fig. 3b). The coordinates of the AHRS platform in the local reference system are: $(x'_A; y'_A; z'_A) = (\text{-}0.5; 0.0; 4.5)$ [m] (Point A in Fig. 2). The sensor measured roll, pitch, yaw and the three translational velocity components with respect to three directions (North, East, Up), which are converted in Gxyz reference system (see Fig. 2) by applying the associated rotation matrices. These data were compared with those from the other sensors installed on-board, including additional accelerometers, inclinometers, load cells and underwater pressure transducers, for cross-checking purposes and real-time sensor diagnostics.

2.2. Data post-processing

The wave-induced dynamics of the system is analyzed in terms of roll, pitch, and heave velocity response amplitude operators (RAOs).

Mathematically, the RAO is a linear, frequency-dependent, complex transfer function between a wave with unitary amplitude and a given phase and the amplitude and phase of the system response. The estimation of the RAOs from experimental data can be carried out in indoor experiments frequency by frequency, by measuring the stationary system response under regular waves of variable frequency, direction, and steepness, or by performing irregular wave tests with large-frequency-range spectra (ideally white noise). The variability of RAOs with wave steepness highlights nonlinear phenomena affecting the structure dynamics. Thus, experimental RAOs must be regarded as linearized indicators depending on the test conditions adopted for their estimation, whose characteristics play a crucial role for the correct characterization of the system dynamics. When irregular wave tests at sea are concerned, the estimation of RAOs is less straightforward, being input spectra narrow-banded. O'Donnel et al. (2020) observed that two methods are indistinguishably used in literature, namely energy spectra method (ESM) and cross-spectral/auto-spectral method (CSM), although they lead to quantitatively different results. ESM estimates RAO's amplitude at a given frequency ω as the square root of a ratio between response (output, E_y) and wave elevation (input, E_η) power spectral densities (PSDs), whereas CSM as the square root of a ratio between output-input cross power spectral density (CPSD), $E_{\eta y}$, and input PSD E_η:

$$\text{a}\Big) RAO_{y,ESM}(\omega) = \left(\frac{E_y(\omega)}{E_\eta(\omega)}\right)^{0.5}$$
$$; \text{b}\Big) RAO_{y,CSM}(\omega)$$
$$= \left(\frac{E_{\eta y}(\omega)}{E_\eta(\omega)}\right)^{0.5}. \tag{1}$$

The practical application of these approaches in sea trials is complicated by the large uncertainty on the real wave conditions acting on the floating structure, and by the impossibility to control other environmental loads that could affect its motions. Hence, waves must be measured at a distance ensuring negligible structure-induced perturbations and full representativeness of the incident wave field at the structure operational position (Boccotti, 2014). This is generally feasible in test sites; however, water depth variations between the wave probes and the floating structure position may induce shoaling and refraction effects modifying the wave directional spectrum. This is inevitable in natural laboratories close to the shore, which are characterized by a significant bathymetric variability, as in the case of the present study (bathymetry map is shown in Fig. 4). In such cases, undisturbed directional wave spectrum in the proximity of the structure may be reconstructed by means of an inverse shoaling-refraction algorithm (Boccotti, 2014) based on the equations

$$E_{\eta,0}(\omega) = C_S(\omega) C_R(\omega) E_\eta(\omega) \tag{2}$$

$$C_S(\omega) = \frac{\tanh(k(\omega)d)[\sinh(2k(\omega)d) + 2k(\omega)d]}{\sinh(2k(\omega)d)} \tag{3}$$
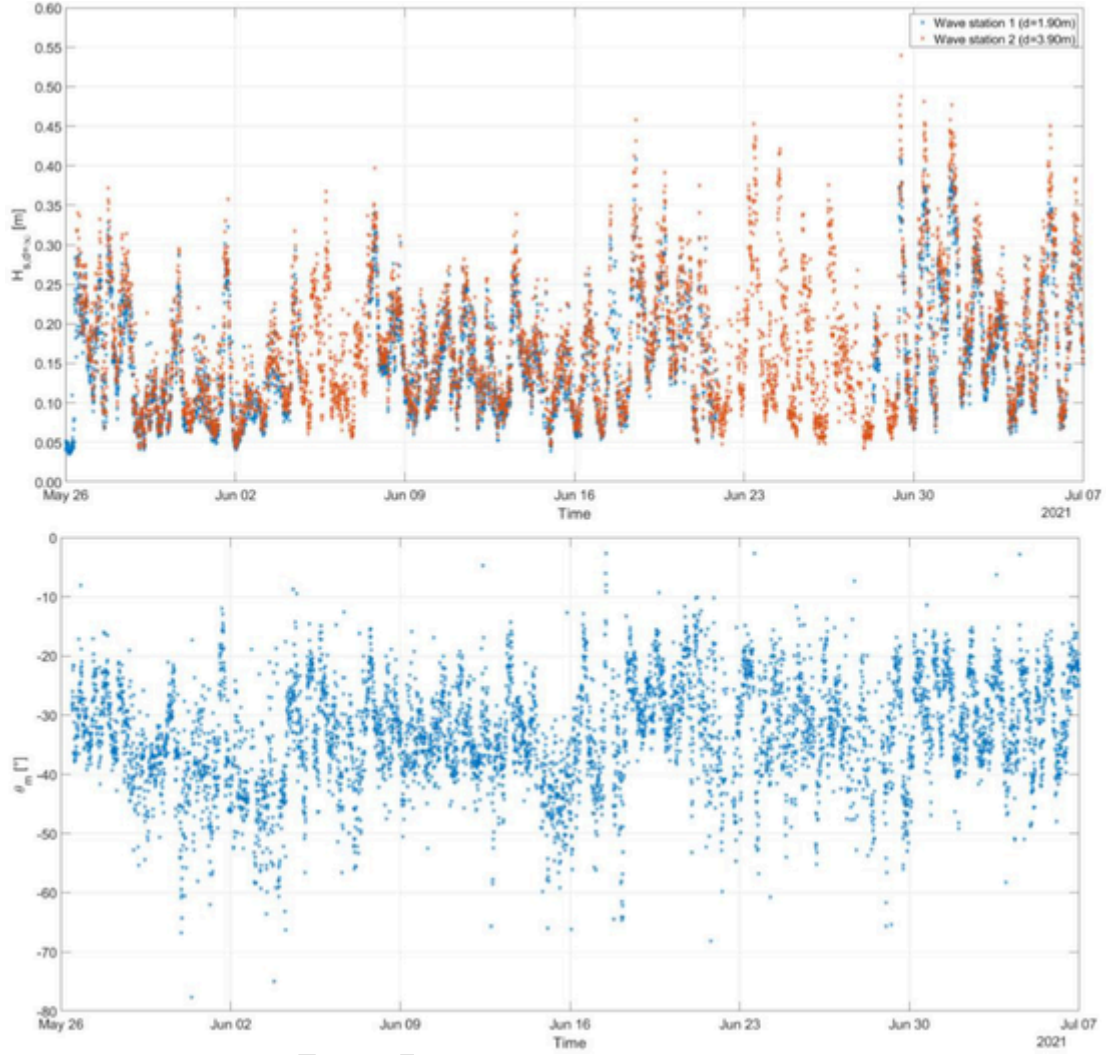
Fig. 5. - Significant wave height (upper panel) and mean wave propagation direction with respect to the North (lower panel) estimated at the structure installation point. Missing points in the plots indicate occasional measurement station disconnection or sensor faults.

Table 3
Input wave classes based on an aggregate classification approach.

Group	Wave class	Mean relative wave angle $\theta_{m,0}$	Significant wave height $H_{s,0}$	Number of records
A	1	-10° to 10°	< 0.15 m	1709
	2	-10° to 10°	0.15 m to 0.30 m	1191
	3	-10° to 10°	0.30 m to 0.55 m	48
B	4	-10° to 10°	0.15 m to 0.20 m	729
	5	-10° to 10°	0.20 m to 0.25 m	327
	6	-10° to 10°	0.25 m to 0.30 m	135
C	7	-10° to 10°	< 0.15 m	1709
	8	-20° to -10°; 10° to 20°	< 0.15 m	382
	9	-30° to -20°; 20° to 30°	< 0.15 m	35

$$C_R(\omega) = \sqrt{\frac{1 - \tanh^2(k(\omega)\,d)\cos^2(\alpha_0(\omega))}{1 - \cos^2(\alpha_0(\omega))}} \tag{4}$$

and

$$\alpha_0(\omega) = \arccos\left(\frac{\cos(\alpha(\omega))}{\tanh(k(\omega)\,d)}\right) \tag{5}$$

being d the water depth of the wave measurement point; E_η the wave elevation power spectral density; k the frequency-dependent wave number; α the frequency dependent mean spectral direction, measured with respect to the line locally orthogonal to the shore; and the subscript "0" denoting deep water conditions. From a physical point of view, C_S is the shoaling coefficient, representing the amplitude modification of each wave component, assumed orthogonal to the shore, while C_R is the refraction coefficient, representing the additional effect induced by wave refraction. Extended description of these phenomena and derivation of Eqs. (3)–(5) can be found in literature (see e.g. (Boccotti, 2014)). Eqs. (2)–(5) are applicable if the bathymetry lines are all straight and parallel to the shore, the slope is relatively small, and the platform is installed on deep waters. These assumptions are acceptable for the present case study, thus justifying the adoption of the method. Since the offshore transposition of the wave phases is not possible, only the amplitude of the RAO has been calculated in the present study. For the same reason, ESM method has been preferred over CSM one for the estimation of the RAOs, being the output-input CPSD $E_{\eta y}$ of less straightforward determination than the input PSD E_η, using the transposition routine.

In principle, individual RAOs for each record can be calculated by directly applying Eq. (1a). However, experimental data show that the input wave energy concentrates on a narrow frequency range, variable from sea state to sea state. Outside this range, spectral values are very
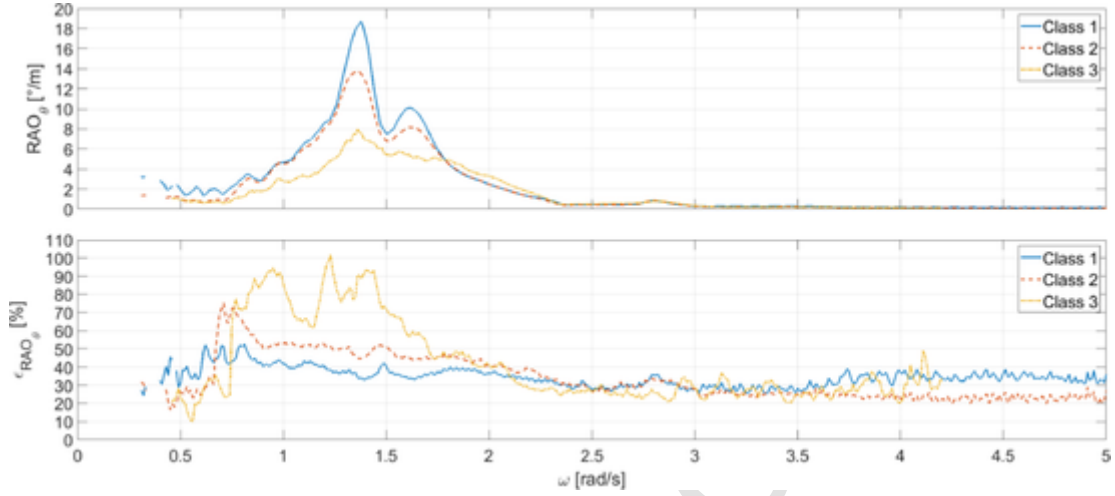
Fig. 6. - Mean pitch RAO and associated uncertainty for input group A. All values refer to 1:15 scale model.

Fig. 7. - Probability density functions of pitch RAO ordinates for input wave group A at the RAO peak frequencies: solid line = estimated from measured data; dashed line = ideal normal distribution.

small, and their estimation is not reliable as it is dominated by measurement and numerical uncertainties, leading to uncertain or even unreasonable values of the associated individual RAO ordinates. To overcome this issue, the application of Eq. (1a) has been limited to frequencies characterized by an input wave spectrum ordinate deemed significant, based on different criteria presented in the following sections. The resulting individual RAOs are therefore relative to a limited frequency range, variable from record to record, and are generally different from each other, due to measurement uncertainty. Finally, the overall RAO estimation is obtained by averaging the filtered individual RAOs available at each frequency (Eq. (6)), within a given sub-set of wave input conditions. The criteria used as input spectrum filtering and classification of the mentioned sub-sets are explained and discussed in Section 3. Although such averaged RAO is the most straightforward outcome of experimental analyses of offshore floating structures, its capability to represent adequately the real system dynamics requires a quantification and characterization of the uncertainty associated with the measure-

ment of the environmental conditions. Herein, the RAO uncertainty is defined as per Eq. (7), where σ_{RAO} is the standard deviation of the available set of individual RAOs for each frequency ω.

$$RAO(\omega) = \frac{1}{N(\omega)} \sum_{i=1}^{N(\omega)} RAO_i(\omega). \tag{6}$$

$$\epsilon_{RAO}(\omega) = \frac{\sigma_{RAO}(\omega)}{RAO(\omega)}. \tag{7}$$

Guidelines for the characterization of uncertainty and for the identification of its sources in the context of experiments on floating structures were provided by the Ocean Engineering Committee of the International Towing Tank Conference (ITTC) (Qiu et al., 2014), which distinguished the cases of model tests, full-scale tests and numerical models. In the present case, the simplified procedures used for the estimation of the input wave spectrum at the platform location and to derive the average of the individual RAOs may be regarded as the main
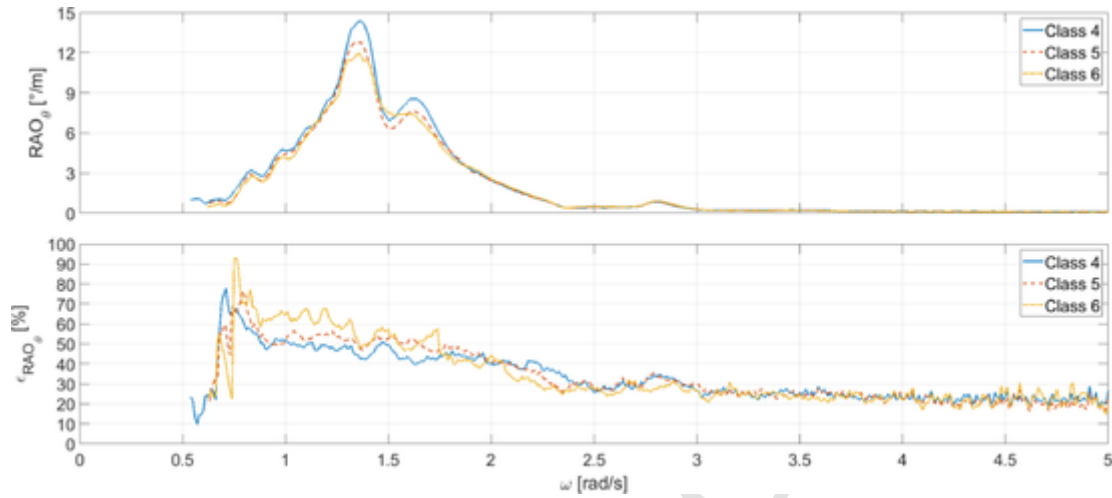
Fig. 8. - Mean pitch RAO and the associated uncertainty for input group B. All values refer to 1:15 scale model.
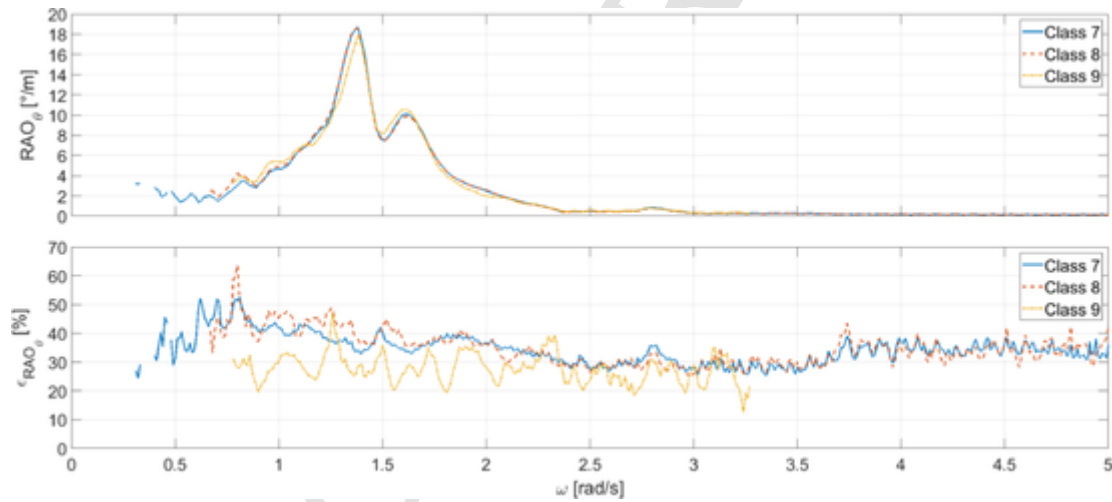
Fig. 9. - Mean pitch RAO and the associated uncertainty for input group C. All values refer to 1:15 scale model.

sources of uncertainty when deriving the RAOs. Other relevant factors include measurement uncertainties, variability of the system dynamic properties (e.g., due to the interaction between local currents and tidal and mooring system), and occurrence of nonlinear phenomena. A key aspect when dealing with an uncertainty analysis is the repeatability of the tests, as it is suggested to apply statistical methods to the results of repeated tests for obtaining reliable estimates. However, test repetition is discouraged in indoor environment due to the high costs and it is impossible at sea: a fact that complicates uncertainty quantification. On the other hand, field tests allow to build up large databases, which allows the selection of the measured data based on the wave spectral properties associated. Since a real sea state can be regarded as a sequence extracted from a stationary ergodic Gaussian random process (Boccotti, 2014), different sea states with similar spectral properties may be regarded as individual realizations of the same process and the uncertainty of any variable linearly related to the wave input will be normally distributed. Therefore, this turns to be an advantage of field tests, if a enough data are collected and a suitable method for sea state classification is identified. Furthermore, if systematic sources of uncertainty (e.g., sensor offset and permanent mooring lines settlings) are excluded, the deviation of the uncertainty distribution from the Gaussian can be used as an indicator of nonlinearities in structure dynamics. Based on these considerations, Section 3 investigates the wave input classification criteria and the related RAO uncertainty values and statistical distributions.

3. Results and discussion

The experimental data presented herein were collected in the first phase of the experiment, involving the base floating platform configuration, between the 26th of May and the 7th of July 2021.

Overall, 5,974 10-minutes records were obtained and analyzed. In this regard, note that the choice of this record length is indeed adequate for recording a stationary sea state at the test site (Boccotti, 2014). For each record, input and output spectra have been calculated based on Welch's method, and RAO analyses have been carried out. All values and figures reported in this section are referred to the 1:15 prototype scale and are to be scaled-up through Froude similarity for getting information about the full-scale system.

For sake of comparison with the experimental results obtained and discussed below, Table 2 shows a list of the theoretical undamped natural frequencies of the prototype structure, obtained through a linearized numerical code (Li et al., 2019).

3.1. Criteria for RAOs estimation

Standard RAO estimation is pursued in a linear framework leading to a quantification dependent on wave frequency and direction. However, experimental data are often well interpreted only through nonlinear models. Therefore, experimental RAO determination must take these elements into account. In the floating body dynamics context, the

Table 4
Input wave classes based on a disaggregate classification approach.

Group	Wave class	Relative wave angle $\theta_0(\omega)$	Spectral ordinate $E_{\eta,0}(\omega)$
D	10	-10° to 10°	1.0e-4m²s/rad to 3.0e-4 m²s/rad
	11	-10° to 10°	3.0e-4m²s/rad to 6.0e-4 m²s/rad
	12	-10° to 10°	6.0e-4m²s/rad to 1.1e-3 m²s/rad
	13	-10° to 10°	1.1e-3m²s/rad to 2.0e-3 m²s/rad
E	14	-40° to -30°; 30° to 40°	1.0e-4m²s/rad to 3.0e-4 m²s/rad
	15	-30° to -20°; 20° to 30°	1.0e-4m²s/rad to 3.0e-4 m²s/rad
	16	-20° to -10°; 10° to 20°	1.0e-4m²s/rad to 3.0e-4 m²s/rad
	17	-10° to 10°	1.0e-4m²s/rad to 3.0e-4 m²s/rad

two major nonlinear hydrodynamic forces are: second- and higher order wave-induced forces, as they involve a transfer of energy between different frequencies, and viscous forces, leading to nonlinear damping. The former effect is quite relevant for the low-frequency surge, sway and yaw motions of soft-moored structures, that often are governed by difference frequency second-order wave loads (Faltinsen, 1993). Therefore, surge, sway, and yaw RAOs would not be reliable indicators of the system response at those frequencies ($\leq$0.15 rad/s, based on estimations from response spectra only). In addition, note that RAOs' experimental estimation would be anyway unreliable as input wave energy content is almost zero at very low (and high) frequencies. Hence, in the present study, the surge, sway, and yaw motions are not investigated, also considering that the prototype's mooring system has been intentionally oversized, as already mentioned. In the studies where these motions are of interest, it is suggested to use other representations of the experimental dynamic response, able to capture nonlinear effects (notable alternatives are described by dos Santos et al. (2020), Katsidoniotaki et al. (2022) and Petromichelakis and Kougioumtzoglou (2021)). Instead, the nonlinear viscous damping does not invalidate the reliability of RAOs as dynamic response indicators, but it causes a peak value variability, depending on the intensity of the excitation. In such cases, experimental RAOs associated with different wave characteristics are expected to be similar in shape but with a different peak value, and may still be used to validate linear (e.g., potential theory based) numerical models, if adequate linearized damping coefficients are used. Finally, it is worth mentioning that other nonlinearities (e.g., due to nonlinear hydrostatic stiffness and/or inertia) could also induce significant alteration of the RAO peak frequencies and shapes, estimated for different input wave characteristics. The manifestation of such phenomena would indicate that the nonlinear representation of system response is essential for its numerical modeling.

Based on the above considerations, two strategies have been investigated for the input wave classification. The first one utilizes "aggregate" sea state properties and is useful for a practical interpretation of the results, while the second uses "disaggregate" spectral properties and reflects closely the RAO definition. Specifically, the word "aggregate" is used in this paper to indicate statistical wave parameters describing the overall characteristics of the sea state (significant wave height and mean propagation direction). Instead, the word "disaggregate" is used to indicate wave parameters associated with a specific spectral frequency (spectral ordinate and spectral direction). In the following, the specific criteria adopted for input wave classification are described, and the corresponding results obtained for pitch motions are presented and discussed. Nevertheless, similar results have been obtained for the other degrees of freedom, but they are not reported in this section for conciseness and since no conceptual or substantial methodological differences can be identified. Finally, a further classification/differentiation based on wind turbine loads (when operating and when not operating) has not been adopted, since it has been observed that their influence on the hull dynamics is negligible, due to the large size of the platform. Such statement is supported by the experimental results of the previous 1:40 tests carried out indoor on a structure model (Ohana et al., 2022), and by the analysis of the experimental data collected during the outdoor campaign, under several turbine operation regimes.

3.1.1. RAOs from aggregate sea state properties

In common engineering applications, design sea states are usually unimodal and are identified by the significant wave height H_s, the mean wave propagation direction θ_m and the frequency spectrum $E(\omega)$, which implicitly includes the other sea state characteristics, such as the peak period T_p and the mean zero-up-crossing period T_z. Therefore, the variability of the system response is assessed as a function of these parameters. To this end, the first wave input classification strategy investigated in this paper is based on aggregate sea state properties, namely H_s, θ_m and, when possible, $E(\omega)$. In this phase, the filtering strategy proposed by Ruzzo et al. (2018) has been adopted for individual RAOs estimation, i.e. data at frequencies where the ordinate of the input (wave) spectrum is smaller than 10 % the corresponding spectral peak, i.e. $S_\eta(\omega) < 0.1\ S_\eta(\omega_p)$, have been discarded. Also, mean RAOs have been estimated only for frequencies where at least 10 individual RAOs are available within the same dataset. The choices of these threshold values resulted from parametric analyses carried out by Ruzzo et al. (2018) on a previous field experiment, and have been confirmed for the present case study by other parametric analyses, whose results are not reported here for conciseness.

For each wave elevation record, the mean wave propagation direction θ_m and the mean spectral directions $\theta(\omega)$ have been estimated at each measuring station by using the methods presented by Boccotti (2014) and Boccotti et al. (2011), respectively. Then, they have been
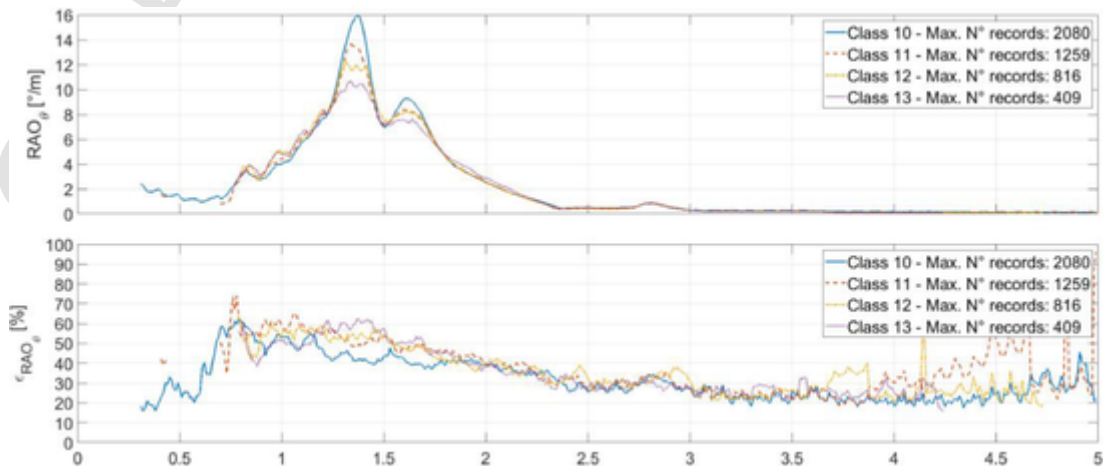
Fig. 10. - Mean pitch RAO and the associated uncertainty for input wave group D. All values refer to 1:15 scale model.
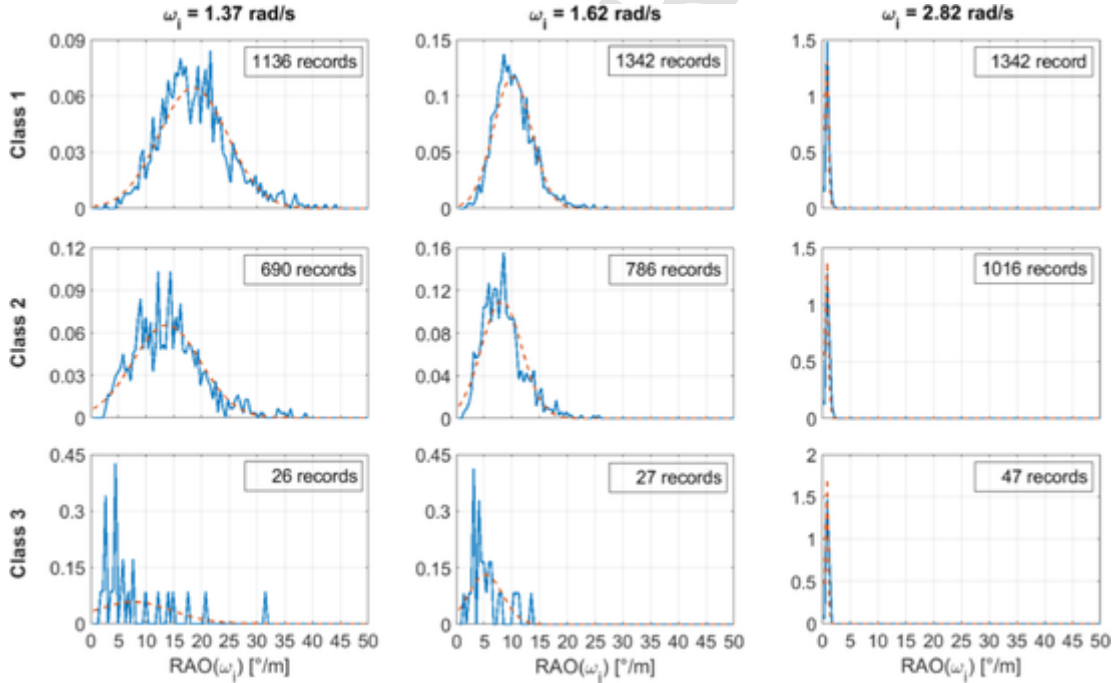
Fig. 11. - Probability density functions of pitch RAO ordinates for input wave group D at the RAO peak frequencies: solid line = estimated from measured data; dashed line = ideal normal distribution.

Fig. 12. - Mean pitch RAO and the associated uncertainty for input wave group E. All values refer to 1:15 scale model.

transposed using Eqs. (2)–(5) to reconstruct the wave spectra at the structure installation point. On a rigorous basis, mean wave propagation direction cannot be transposed without referring to the directional spectrum. However, an approximate estimate is obtained by Eq. (5) by assuming a frequency ω equal to the peak frequency ω_p of the sea state. This fact is not expected to lead to inconsistent estimates, as only data measured by the deepest wave station ($d = 3.90$ m) are processed by this algorithm, which is reliable in deep waters conditions. Finally, significant wave height is estimated from the transposed spectra, as reported in Eq. (8). Results are shown in Fig. 5.

$$H_{s,0} = 4\sqrt{\int_0^\infty E_{\eta,0}(\omega)\,d\omega}. \tag{8}$$

It is seen that the results from the two stations in terms of transposed significant wave height are highly consistent with each other. Quantitatively, the mean difference between the transposed values (computed

when both records are available) is of about 0.014 m (6.9 %), while its standard deviation is of about 0.020 m (15.0 %), validating the applicability of the inverse shoaling-refraction algorithm. Maximum estimated $H_{s,0}$ is about 0.54 m, which is associated with a full-scale value of 8.1 m. The mean wave propagation direction varies, but not substantially, remaining approximately orthogonal to the fore side of the structure. In detail, considering the yaw motion, the x-axis orientation oscillates indeed between -45° and -30° with respect to the North, resulting in relative angles between waves and structure often within ±10° (mean relative angle = -3.6°; standard deviation = 8.5°). The mean relative wave angle and the significant wave height are the two aggregate parameters chosen for the input sea state classification, as shown in Table 3, where nine input wave classes, arranged in three groups, are proposed. Each group explores the effects of the variability of one of the two parameters within a given range, with the other fixed within a given set of values correspondent to the greatest availability of data measured.
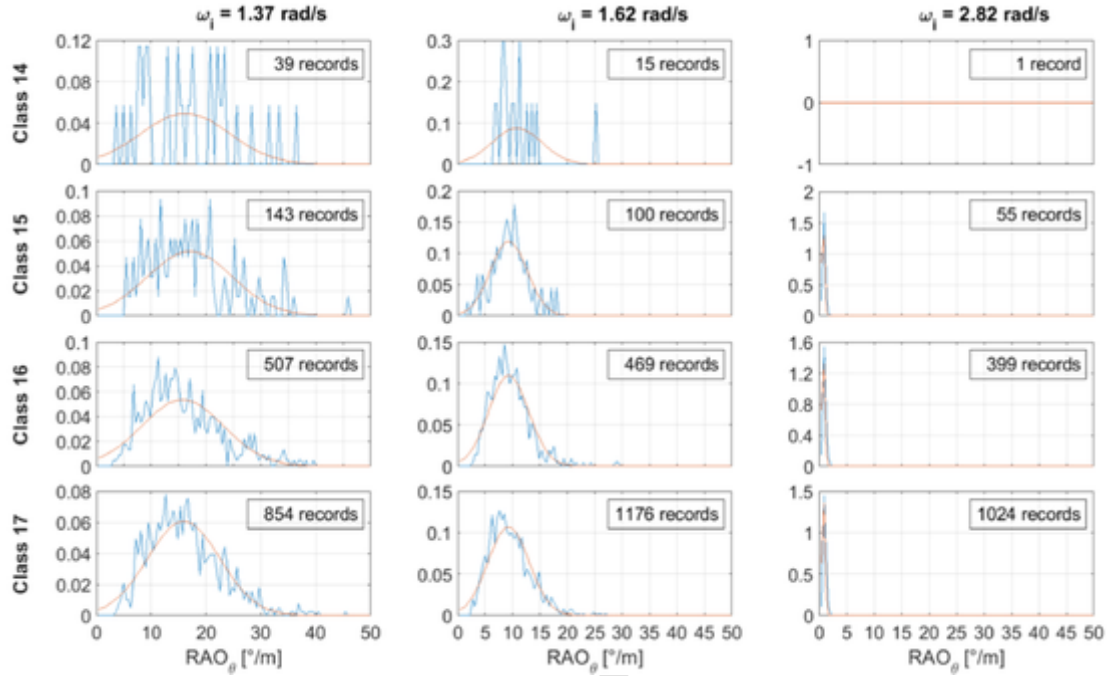
Fig. 13. - Probability density functions of pitch RAO ordinates for input wave group E at the RAO peak frequencies: solid line = estimated from measured data; dashed line = ideal normal distribution.

Table 5
Input wave classes based on optimized hybrid classification approach.

Group	Wave class	Relative wave angle $\theta_0(\omega)$	Significant wave height $H_{s,0}$
F	18	-20° to 20°	0.00 m to 0.10 m
	19	-20° to 20°	0.10 m to 0.20 m
	20	-20° to 20°	0.20 m to 0.30 m
	21	-20° to 20°	0.30 m to 0.55 m

Fig. 6 shows the mean pitch RAOs and the associated uncertainty, obtained for input group A (wave classes 1-3). Mean pitch RAO for Class 1 is characterized by two main peaks at about $\omega_1 = 1.38$ rad/s and $\omega_2 = 1.62$ rad/s, followed by a minor peak at about $\omega_3 = 2.82$ rad/s. The first two frequencies reflect the natural (coupled) heave and pitch natural frequencies, while the third one highlights one of the moonpool natural frequencies. The main impact of an increased $H_{s,0}$ on the mean pitch RAO is the reduction of the peaks. As a secondary effect, the first peak frequency is also reduced to $\omega_1 = 1.33$ rad/s for class 2 and to $\omega_1 = 1.32$ rad/s for class 3. Both the reduction of the peaks' magnitude and the slight reduction of the peak frequencies are consistent with larger viscous damping forces, linked to the large platform motion responses. Similar conclusions can be drawn by considering the RAO uncertainty. Indeed, it is proportional to H_s in the frequency range of interest, thus denoting a greater scatter of individual RAO values in case of more severe load cases.

Although the uncertainty is a quantitative indicator of the reliability of a RAO estimate, it is of great interest to provide qualitative indicators as well, and to quantify the impact of the criterion chosen for input wave classification. This is an important point considering the scarcity of reference studies on RAO uncertainty characterization from field experiments in literature. In this context, Fig. 7 shows the RAO's probability density functions (PDFs) computed for each input wave class at the three RAO peak frequencies. The experimental PDFs are compared to ideal normal distributions computed by imposing that both distributions have the same mean and standard deviation values. Reasonable agreement between the distributions is obtained for Classes 1 and 2. Specifically, a slight systematic asymmetry is observed, i.e., around the peak frequencies the normal distribution tends to overestimate the

probability density at large RAO values, and to underestimate it at small ones. The opposite behavior is observed at the tails, where the normal distribution tends to underestimate the probability density of the maximum RAO's values and to overestimate those of the minimum ones. This is consistent with the observed nonlinearities. Data pertaining to input wave Class 3 are not sufficient to determine a reliable probability density function estimate. In this context, available data show that the mentioned asymmetry increases, consistently with the expected increased effects of nonlinear damping.

To reduce the uncertainty, several alternative classification criteria have been investigated, based on the "aggregate wave parameters" approach. Since very restrictive criteria result in less populated datasets, which in turn lead to poorer estimations, it is necessary to find compromises based on the comparison of RAO and uncertainty estimates. For illustration purposes, the RAOs and the associated uncertainties obtained for input groups B (wave classes 4-6) and C (wave classes 7-9) are shown in Figs. 8 and 9, respectively, and discussed below.

Input group B is class 2 of group A, divided in three classes (4-6) with increasing significant wave height. This definition allows investigating if RAO uncertainty could be reduced by refining the sampling of input sea states depending on H_s only. It is worth noticing that the results are quite similar to those relative to group A, irrespective of the reduced input variability. Indeed, increasing H_s values lead to a RAO peak reduction and to a wider uncertainty. Compared to class 2, relatively small differences are observed also from a quantitative point of view. Considering for instance the first RAO peak value, the maximum difference is observed for class 6, i.e., -12.8 %, while class 4 shows an increase of 4.7 %. Instead, the uncertainty slightly reduces for class 4, it is almost identical for class 5, and it increases for class 6. From a physical point of view, this is consistent with the manifestation of nonlinear damping: higher waves induce larger damping forces resulting in reduced mean RAOs (more so around the natural frequencies) with an increased scatter, due to the non-linear nature of viscous forces, and thus uncertainty. From a classification point of view, it may be concluded that considering a narrower range of significant wave heights, within an input class, results in marginally more accurate mean RAO estimate, without significantly affecting the uncertainty. From a practical point

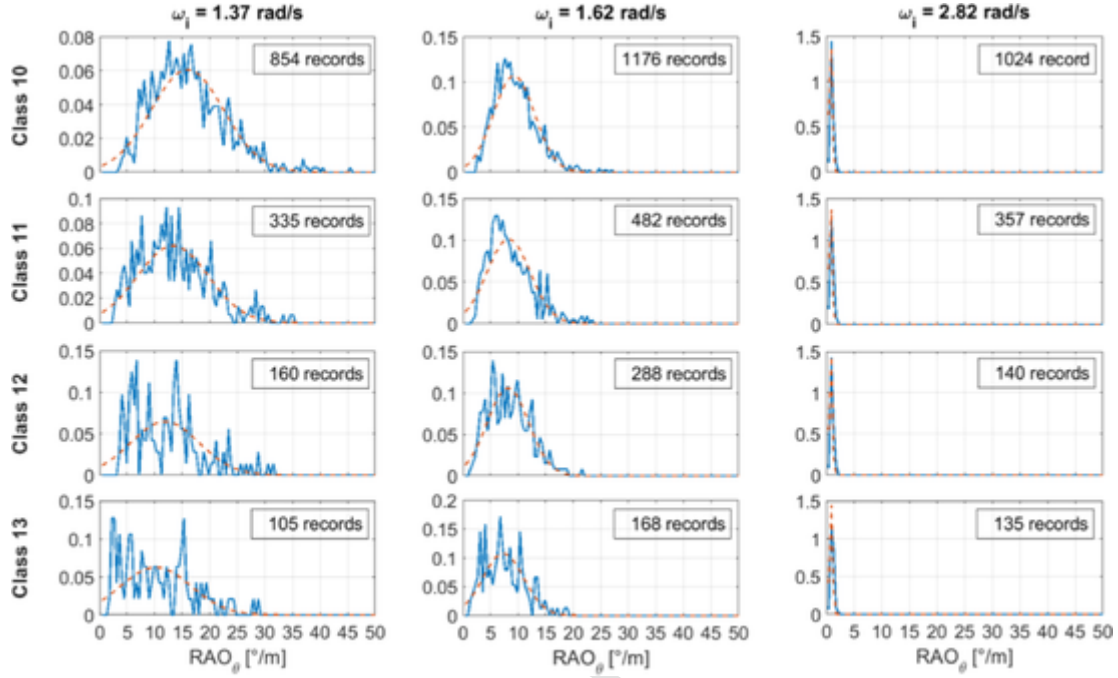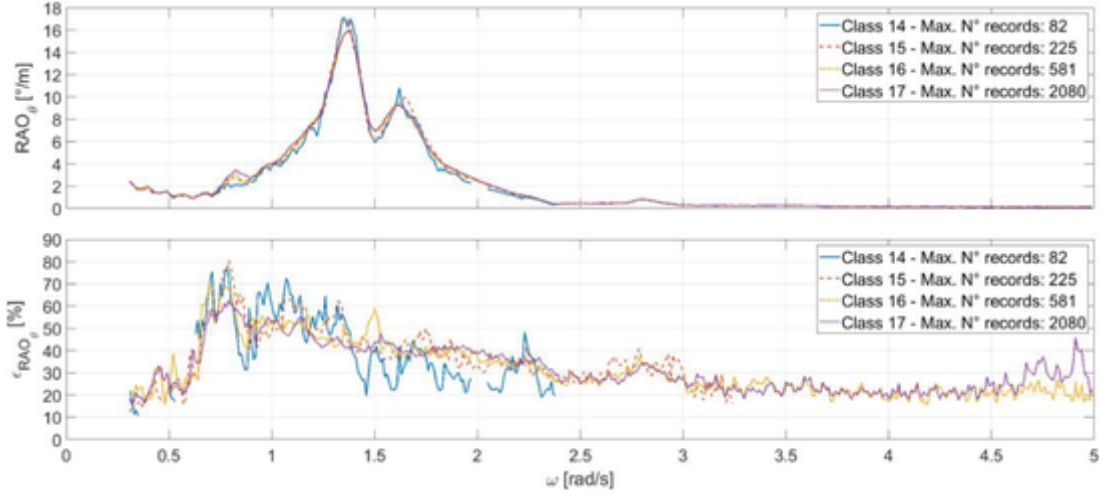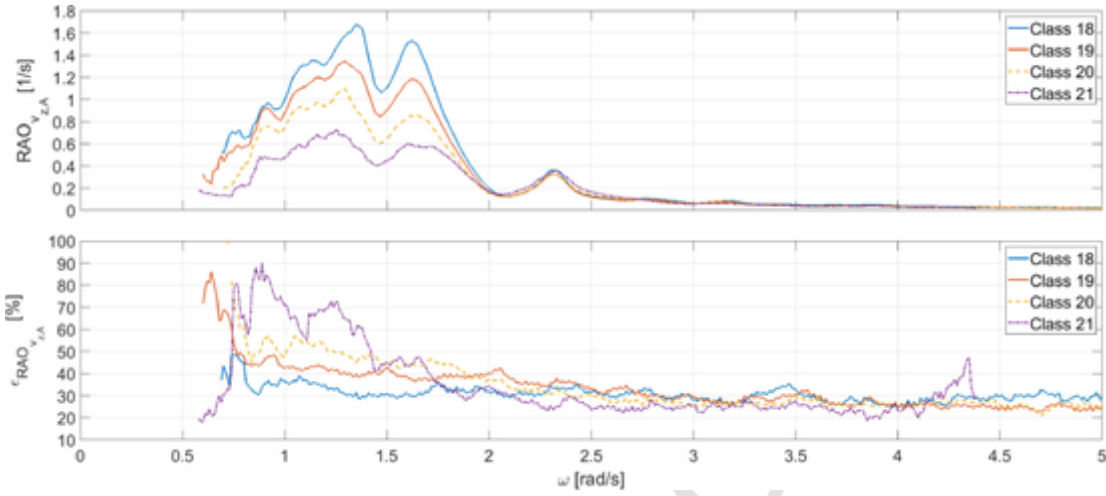**Fig. 14.** - Mean heave velocity RAO in Point A and the associated uncertainties for input wave group F. All values refer to 1:15 scale model.
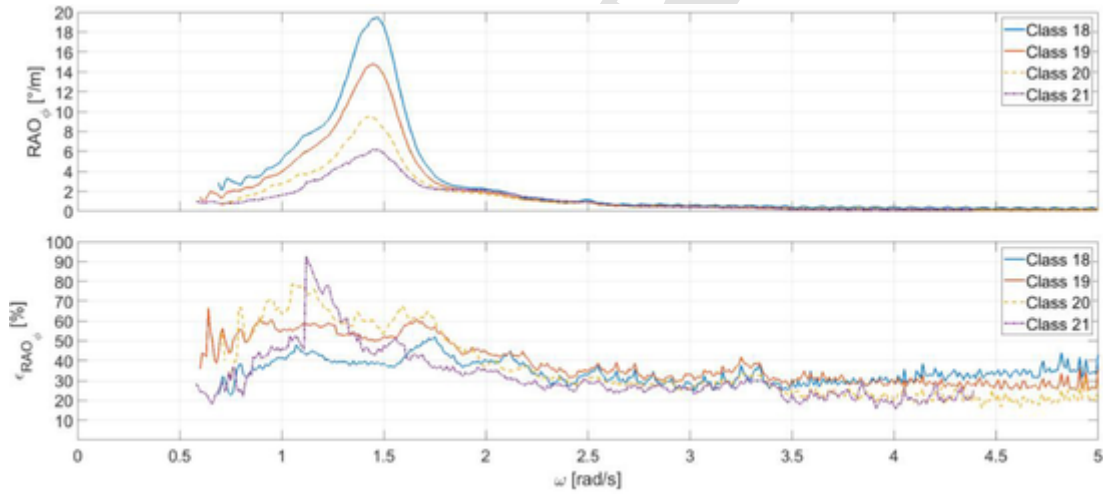

Fig. 15. - Mean roll RAO and the associated uncertainties for input wave group F. All values refer to 1:15 scale model.

of view, if a classification criterion based on aggregate wave properties is adopted, it is hence suggested to give priority to the number of records per class, crucial the determining the RAO's PDFs, rather than considering narrower significant wave height ranges.

Input group C (wave classes 7-9) is aimed at investigating RAO and uncertainty estimates variability with mean input wave direction. The smallest H_s range is used to minimize nonlinear effects and to simplify the comparison with input class 1 (coinciding with class 7). From a holistic perspective, it is seen that the mean wave direction has overall a negligible effect on the results within the range measured during the experiment.

3.1.2. RAOs from disaggregate sea state properties

Although the classification abovementioned, based on aggregate wave parameters, is consistent and convenient for the interpretation of the experimental data, it has some intrinsic limitations. Indeed, incident sea states can be made up of two or more wave families, each with its own frequency and propagation direction ranges. More precisely, small sea states usually present a great variety of spectra, including multi-modal ones, made up of swells superimposed to (locally generated) wind waves. In such cases, aggregate wave parameters may fail to properly characterize the sea state properties. A potential alternative is to further refine the classification criteria by introducing additional parameters, e.g., depending on spectrum shape. This approach, being more selective, would support the automatized identification of similar

sea states, but would lead to classes composed of few samples. To deal with this issue, an analysis based on the individual RAO values associated with a specific frequency and direction is proposed. This disaggregate approach reflects better the RAO definition and is applicable as long as energy transfer between different frequencies due to nonlinear effects (e.g., difference-frequency loads) is neglected. Based on the available experimental data, other two groups, each made up of four classes, have been identified, and the corresponding RAOs and uncertainties have been estimated by applying Eqs. (6) and (7). Each class j, at each frequency ω, is made up of the sea states i such that:

$$\left\{ \left[\theta_0 \left(\omega \right) \right]_i \in \left[\Delta \theta_0 \right]_j \right\} \, \wedge \, \left\{ \left[E_{\eta,0} \left(\omega \right) \right]_i \in \left[\Delta E_{\eta,0} \right]_j \right\}. \tag{9}$$

The parameters adopted for each class are reported in detail in Table 4. It can be observed that a larger range of input wave propagation directions can be investigated with respect to the aggregate approach. Indeed, waves with a larger relative propagation angle recorded at the test site, generally associated with secondary wave families, are not included in the classes by considering mean wave propagation direction only. This may lead to potentially misleading input classes, each including wave spectral components with quite different propagation directions.

Fig. 10 shows mean pitch RAOs and the associated uncertainties calculated for input group D (wave classes 10-13), i.e., considering only spectral ordinates with small relative angles with respect to the
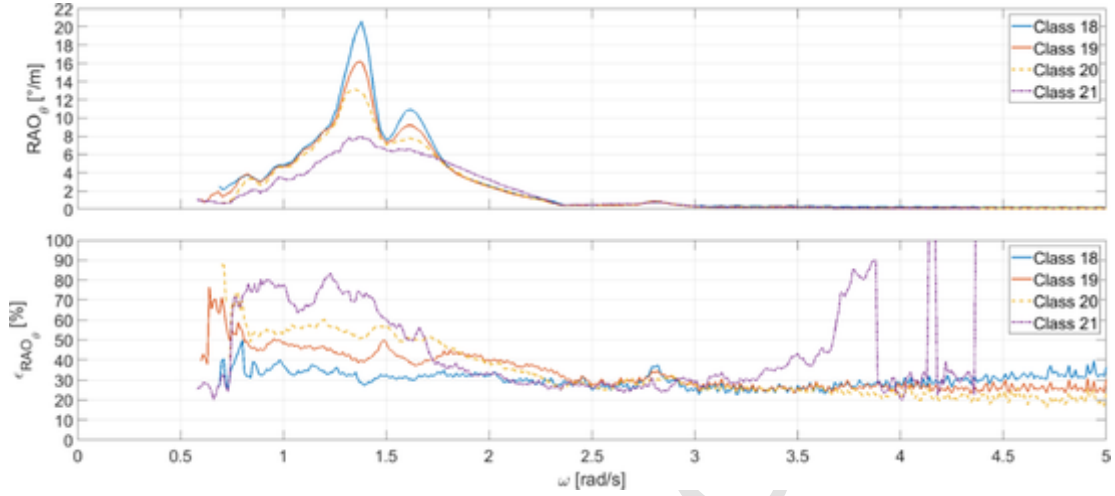
Fig. 16. - Mean pitch RAO and the associated uncertainties for input wave group F. All values refer to 1:15 scale model.
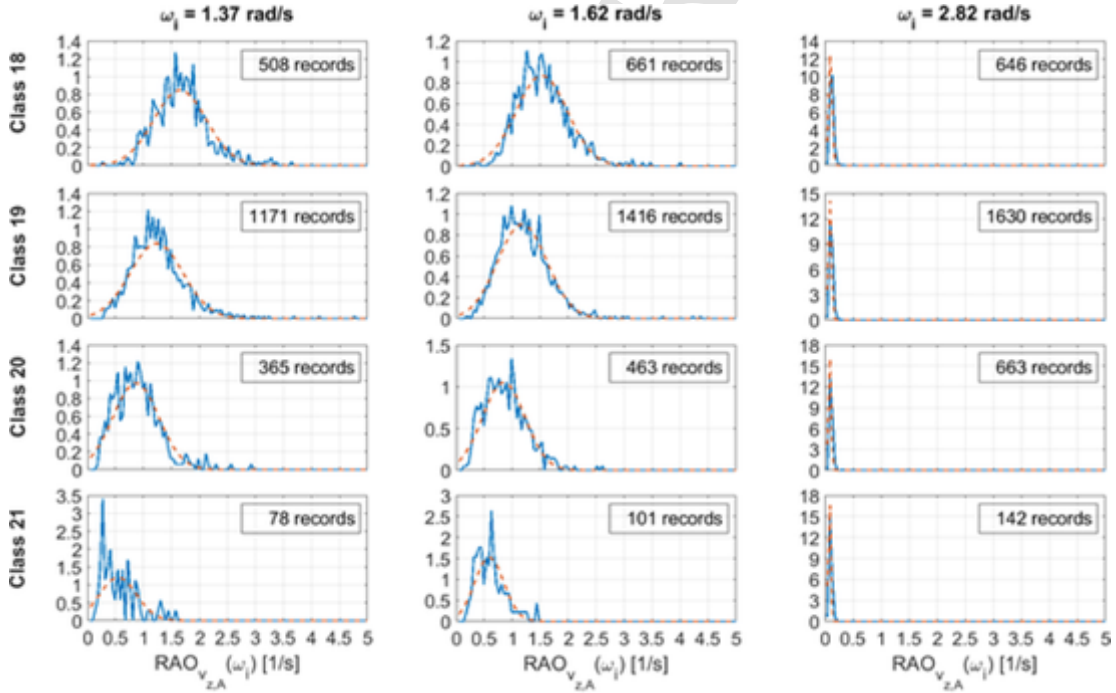
Fig. 17. - Probability density functions of heave velocity (Point A) RAO ordinates for input wave group F at the RAO peak frequencies: solid line = estimated from measured data; dashed line = ideal normal distribution.

platform. Fig. 11 shows the probability density function of the RAO ordinates, estimated for the same input wave classes at the three RAO peak frequencies, compared with the associated ideal normal distribution. It can be observed that the overall results are comparable to those obtained for the input wave groups A-B, i.e., mean RAO decreases in the vicinity of the peaks for larger input waves, and its uncertainty increases accordingly. Hence, the nonlinear effect identified for increasing H_s based on the proposed aggregate analysis approach, applies also to the disaggregate approach, i.e., for increasing spectral ordinates. This provides another clue in favor of the physical interpretation proposed, related to the importance of the nonlinear viscous damping. However, the variability between the different RAO estimates within group D is smaller with respect to group A. This can also be observed for other input wave classes. Such behavior could be explained by considering that the disaggregate sampling approach reduces the variability of averaged H_s between the input classes. Considering for instance ω = 1.37 rad/s in Figs. 11, averaged H_s of the sea

states included in Classes 10-13 are 0.16 m, 0.21 m, 0.23 m and 0.26 m, respectively. It follows that the RAO depends on both the input wave spectral ordinate around its frequency and the overall first-order wave spectrum momentum, due to nonlinear effects. Hence, a classification based on spectral ordinates, would neglect the latter dependence, leading to an underestimation of the nonlinear effects. This statement is supported also by the analysis of uncertainty distributions. Indeed, uncertainty distributions of Classes 12-13 appear not only to deviate from normal distribution, but also to have separate peaks associated with sets of sea states with similar spectral ordinates but different H_s. This fact confirms that the disaggregate sampling approach may introduce inaccuracies for severer wave conditions, due to the increasing importance of nonlinearities. In such conditions, the adoption of a suitable aggregate approach is recommended.

Finally, Fig. 12 shows the mean pitch RAOs and the associated uncertainties for input group E (wave classes 14-17) and Fig. 13 shows the corresponding uncertainty distributions. It is seen that the impact of the

Fig. 18. - Probability density functions of roll RAO ordinates for input wave group F at the RAO peak frequencies: solid line = estimated from measured data; dashed line = ideal normal distribution.
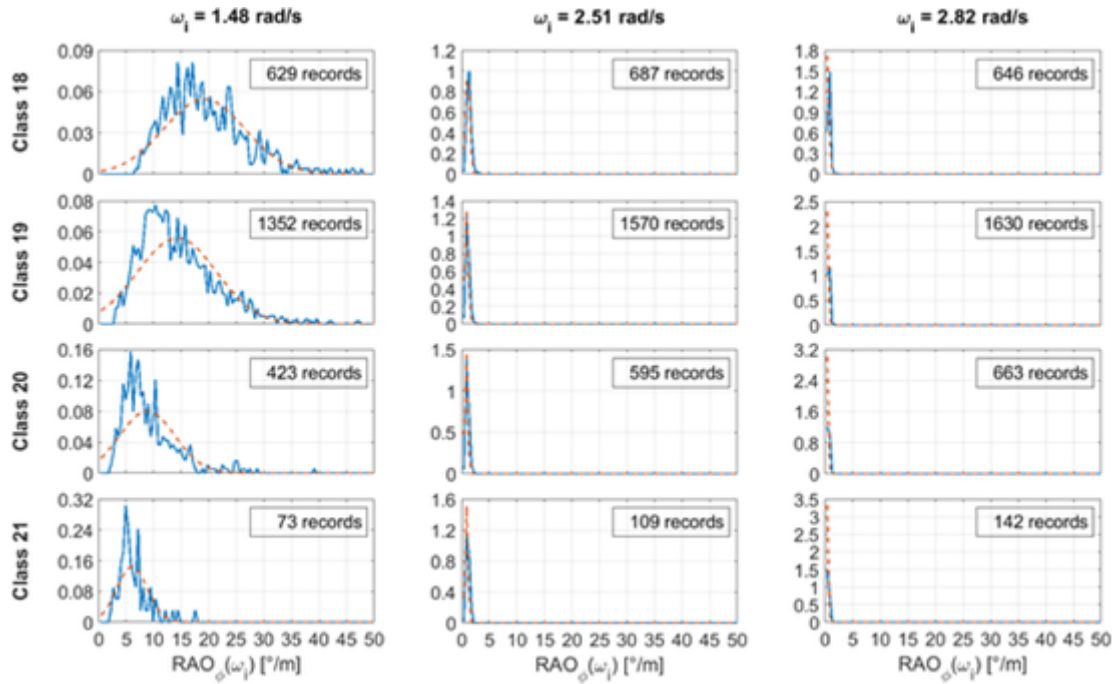
disaggregated wave spectral propagation direction on the results is small. Specifically, it can be deemed completely negligible for relative angles within ±20°, while more oblique waves slightly amplify RAO peaks and separate the first one in two close but distinct peaks. Although small, this amplification and the corresponding peak's separation repeat systematically for oblique waves also for other classes, not reported for brevity. Physical justification for these effects may be found in the small asymmetries observed in the mass and mooring system properties of the prototype. Overall, however, the results show that structure response does not change significantly over a range of relative propagation angles around $-30° < \theta_0(\omega) < 30°$. Furthermore, it is seen that the disaggregate input sampling approach allows to explore a larger range of wave propagation directions with respect to the aggregate one, more compatibly with the real input wave directionality.

In conclusion, it is seen that the aggregate input sampling approach is more feasible for practical applications, since it better captures the nonlinear dynamic effects, and its results are easier to be interpreted and exploited for validation purposes. However, it does not allow dealing properly with wave directionality, especially when mixed input sea states occur. Thus, it is suggested to complement it with the disaggregate approach, at least in the form of a filter, to exclude from the analysis input spectral components whose relative propagation direction is significantly different from the mean one. Finally, based on the parametric analysis carried out, it is suggested to calibrate input sampling to have at least 75-100 records available for each class, and therefore to allow a sufficiently good reconstruction of the uncertainty distribution.

3.2. Experimental structure dynamics

Based on the conclusions of Section 3.1, a hybrid classification approach is adopted for the analysis of the experimental data, i.e., the input wave intensity is classified using the significant wave height H_s (aggregate parameter approach), while the wave directionality is considered through the spectral wave propagation direction at each frequency (disaggregate parameter approach). The associated input wave classes are shown in Table 5, aimed at minimizing the nonlinear effects within each input wave class, while preserving the minimum number of records required to characterize the uncertainty distribution.

Response amplitude operators (RAOs) of heave velocity at point A (Fig. 2), roll and pitch for the input wave group F are shown in Figs. 14, 15 and 16 in conjunction with the associated uncertainties. Results in all the degrees of freedom are very consistent between each other, in terms of RAO shapes, peak frequencies and nonlinearities. An important heave-pitch coupling is observed, as expected, due to the structure asymmetry with respect to the y-axis. Instead, roll is decoupled from the other degrees of freedom since the structure is symmetric with respect to the x-axis. The couplings between the floating body motions and the moonpool modes are limited, resulting in small rigid body motions at high frequencies. In detail, the following moonpool frequencies appear: $\omega_{m,1}$ = 2.32 rad/s in heave velocity RAO, 2.49 rad/s in roll RAO and 2.80 rad/s in pitch RAO. It should be noted that such couplings are more significant in heave velocity RAO (Fig. 14), since velocity RAOs are amplified by a factor ω with respect to the motion RAOs, enhancing the high-frequency contributions. It follows that the high-frequency motions induced by the moonpool forces are negligible, but the corresponding contributions in velocity and acceleration spectra may be significant. The peak frequencies of the coupled heave and pitch RAOs, representative of the natural frequencies of the corresponding modes, are ω_1 = 1.35-1.38 rad/s and ω_2 = 1.62 rad/s for the smallest input waves. The corresponding peak frequency of roll RAO is ω_3 = 1.47 rad/s. As the input significant wave height increases, RAO peak ordinates in all the degrees of freedom reduce due to nonlinear damping, becoming hardly distinguishable for higher H_s values. Correspondingly, measured peak frequencies are also slightly altered due to small nonlinear variations in the system dynamic properties. In general, the estimated quantitative RAO values can be used to tune numerical models, e.g., by assigning a linearized damping matrix dependent on the input wave parameters. Some notable experimental observations are that the moonpool-induced RAO peaks look less sensible to input H_s, thus denoting in a first instance that linear damping lid models may be deemed admissible for the representation of the moonpool dynamics. Finally, the maximum amplitudes of roll and pitch motions are comparable, despite the relative wave propagation angles are close to the x-axis. This fact was further investigated by conducting a comparative analysis against data from other sensors installed on-board (accelerometers, inclinometers, and submerged pressure transducers).
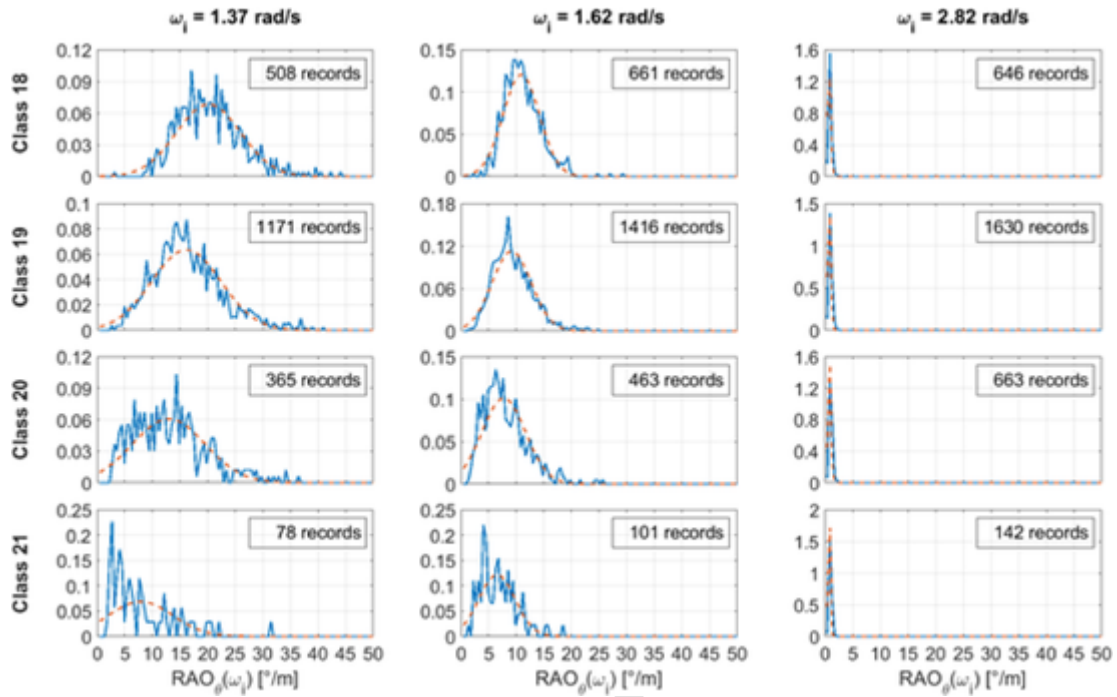
Fig. 19. - Probability density functions of pitch RAO ordinates for input wave group F at the RAO peak frequencies: solid line = estimated from measured data; dashed line = ideal normal distribution.

This analysis confirmed the occurrence of non-negligible roll motions for small relative wave propagation angles, regardless of the amplitude of the range of input wave directions considered. As previously mentioned, the reasons for this unexpected behavior might be ascribed to the asymmetries observed in the mass and mooring system properties of the prototype, which need to be further investigated.

It can be observed that the optimized hybrid classification method has resulted in a slight reduction of the uncertainty, which is between 30-60 % for $H_s < 0.30$ m. As mentioned in the previous section, these relatively high values and the increase with H_s are expected, due to the nonlinear effects. However, the analysis carried out confirms the robustness of mean RAO estimates, which is consistent throughout the whole set of considered wave classification criteria. Uncertainty distributions for all the degrees of freedom are shown in Figs. 17, 18 and 19.

Results are again consistent with those shown in the previous Section, i.e., the experimental curve deviations from ideal normal distributions are relatively small for smaller waves and increase with H_s due to the nonlinear effects. However, a visible asymmetry of the first roll RAO peak distribution is observed also for relatively small waves (input wave class 19), confirming the above-mentioned observation about intrinsic nonlinearities involved in the roll motion.

4. Conclusions

This article has described the results of an intermediate-scale field experiment of a novel multi-purpose floating platform, designed to host aquaculture and renewable energy production from wind and wave energy devices. The platform concept was introduced in the context of "The Blue Growth Farm" H2020 EU project (Lagasco et al., 2019; BGF project website). The project included the testing of a 1:15 model at the Natural Ocean Engineering Laboratory (NOEL) of Reggio Calabria (Italy). The results considered in the present work are based on data recorded between May and July 2021. Froude similarity was used for scaling the structural mass and geometry, and the local met-ocean conditions were interpreted as design conditions for the prototype technologies (performance scaling approach). The system rigid body dynamic response has been identified deriving the mean Response Ampli-

tude Operators (RAOs) estimated by combining the input (irregular sea waves) and the output (rigid body motions) measured data.

This article has proposed a methodology for performing such RAO estimations. Specifically, the proposed method is based on averaging the results obtained from individual input sea states, adequately partitioned in consistent groups. This approach provides quantitative results useful for the tuning of linearized numerical models and gives an insight into the nonlinearities involved in the system dynamics. Two different approaches for input wave classification have been proposed and compared. Specifically, a distinction based on aggregate input sea state properties (e.g., significant wave height) has been identified as the optimal choice if it is complemented by a filter based on disaggregate spectral wave propagation direction. This approach simplifies the interpretation and use of the results, while guaranteeing a good representation of both wave directionality and system dynamics nonlinearities. Quantitative and qualitative information about the methods of analysis of the total RAO uncertainty and its distribution have been also provided, as well as recommendations to reduce it in practical applications. It has been shown that the deviation from a normal distribution may be used as an indicator of appropriateness of the selected input wave classes, if a sufficient number of records is available. As a practical reference value, at least 75-100 sea states must be available for each class, even at the cost of increasing the scatter of the input wave properties considered.

Based on the identification method proposed, the dynamic behavior of the proposed floating platform concept in heave, roll and pitch motions has been investigated. The analysis has considered the base structure configuration, operating without wave energy converters and aquaculture cage models. The results have allowed identifying key characteristics of the system, although relatively high total uncertainties have been measured (30-80%). RAO peak frequencies and amplitudes have been obtained for variable input significant wave heights and may be used for numerical model validation. Significant nonlinear damping effects have been observed in all the degrees of freedom, resulting in dramatic peak RAO reductions (up to -68% within the considered input wave classes) and in strong deviations of uncertainty distributions from the normal probability density functions for severer wave

conditions. Nonlinearities are also responsible of the relatively high uncertainty of mean RAO estimations. Heave, roll, and pitch motions are substantially decoupled from moonpool dynamics, while non-negligible couplings are expected to be found in velocity-acceleration RAOs, at least for heave-pitch degrees of freedom. Finally, roll is decoupled from heave and pitch, but its maximum amplitude is relatively high even for waves parallel to the structure, potentially due to scaling inaccuracies and asymmetries in the prototype mass distribution and mooring system properties.

Future work will focus on the analysis of the coupled dynamic behavior of the platform including all the relevant technologies, and the implementation and validation of coupled numerical codes, considering the asymmetries and the nonlinearities that emerged experimentally. Furthermore, based on the experimental data, specific studies on the moonpool dynamics will be undertaken, considering its relevance for aquaculture installations and for the quantification of high-frequency inertial loads on structure components. The dynamic behavior of mooring lines, wind turbine, and WECs will be investigated as well.

Declaration of Competing Interest

The authors declare that they have no known competing financial interests or personal relationships that could have appeared to influence the work reported in this paper.

Data Availability

Data will be made available on request.

Acknowledgments

References

[Abhinav et al., 2020]   K.A. Abhinav, M. Collu, S. Benjamins, H. Cai, A. Hughes, B. Jiang, S. Jude, W. Leithead, C. Lin, H. Liu, L. Recalde-Camacho, N. Serpetti, K. Sun, B. Wilson, H. Yue, B.-Z. Zhou, Offshore multi-purpose platforms for a Blue Growth: a technological, environmental and socio-economic review, Sci. Total Environ. 734 (2020) 138256, https://doi.org/10.1016/j.scitotenv.2020.138256.

[Arena and Barbaro, 2013]   F. Arena, G. Barbaro, The natural ocean engineering laboratory, NOEL, in Reggio Calabria, Italy: a commentary and announcement, J. Coast. Res. 290 (2013) vii–x, https://doi.org/10.2112/13A-00004.

[Bak et al., 2013]   C. Bak, F. Zahle, R. Bitsche, T. Kim, A. Yde, L.C. Henriksen, M.H. Hansen, J.P.A.A. Blasques, M. Gaunaa, A. Natarajan, The DTU 10-MW Reference wind Turbine. Danish Wind Power Research, Trinity, Fredericia, Denmark, 2013.

[Boccotti, 2014]   P. Boccotti, Wave Mechanics and Wave Loads on Marine Structures, Butterworth-Heinemann (Elsevier), Oxford, 2014 doi.org/10.1016/C2013-0-13663-X.

[Boccotti, 2003]   P. Boccotti, On a new wave energy absorber, Ocean Eng. 30 (2003) 1191–1200, https://doi.org/10.1016/S0029-8018(02)00102-6.

[Boccotti et al., 2011]   P. Boccotti, F. Arena, V. Fiamma, A. Romolo, G. Barbaro, Estimation of mean spectral directions in random seas, Ocean Eng. 38 (2011) 509–518, https://doi.org/10.1016/j.oceaneng.2010.11.018.

[Clarke and Bostock, 2017]   R. Clarke, J. Bostock, Regional Review on Status and Trends in Aquaculture Development in Europe - 2015, Food and Agriculture Organization of the United Nations (FAO), Rome, Italy, 2017.

[dos Santos, Brudastova and Kougioumtzoglou, 2020]   K.R.M. dos Santos, O. Brudastova, I.A. Kougioumtzoglou, Spectral identification of nonlinear multi-degree-of-freedom structural systems with fractional derivative terms based on incomplete non-stationary data, Struct. Saf.

86 (2020) 101975, https://doi.org/10.1016/j.strusafe.2020.101975.

[European Commission, Directorate-General for Maritime Affairs and Fisheries 2019]   European Commission, Directorate-General for Maritime Affairs and Fisheries, The EU Blue Economy Report 2019, Publications Office, 2019, https://doi.org/10.2771/21854.

[Faltinsen, 1993]   O.M. Faltinsen, Sea Loads on Ships and Offshore Structures, Cambridge University Press, Cambridge, UK, 1993.

[Fontanella et al., 2019]   A. Fontanella, F. Taruffi, S. Muggiasca, M. Belloli, Design methodology for a floating offshore wind turbine large-scale outdoor prototype, in: Proceedings of the ASME 2019 38th International Conference on Ocean, Offshore and Arctic Engineering ASME, Glasgow, Scotland, UK, 2019, https://doi.org/10.1115/OMAE2019-95979.

[Jouffray et al., 2020]   J.-B. Jouffray, R. Blasiak, A.V Norström, H. Österblom, M. Nyström, The blue acceleration: the trajectory of human expansion into the ocean, One Earth 2 (2020) 43–54, https://doi.org/10.1016/j.oneear.2019.12.016.

[Katsidoniotaki, Psaros and Kougioumtzoglou, 2022]   M.I. Katsidoniotaki, A.F. Psaros, I.A. Kougioumtzoglou, Uncertainty quantification of nonlinear system stochastic response estimates based on the Wiener path integral technique: a Bayesian compressive sampling treatment, Probabilistic Eng. Mech. 67 (2022) 103193, https://doi.org/10.1016/j.probengmech.2021.103193.

[Lagasco et al., 2019]   F. Lagasco, M. Collu, A. Mariotti, E. Safier, F. Arena, T. Atack, G. Brizzi, P. Tett, A. Santoro, S. Bourdier, F. Salcedo Fernandez, S. Muggiasca, I. Larrea, New engineering approach for the development and demonstration of a multi-purpose platform for the blue growth economy, in: Proceedings of the ASME 2019 38th International Conference on Ocean, Offshore and Arctic Engineering ASME, Glasgow, Scotland, UK, 2019, https://doi.org/10.1115/OMAE2019-96104.

[Lee et al., 2021]   J. Lee, F. Zhao, A. Dutton, B. Backwell, L. Qiao, W. Lang, E. Clarke, A. Lathigara, M. Shardul, M. Smith, D. Younger, T.W. Han, L. Abreu, Global Offshore Wind Report 2021, Global Wind Energy Council (GWEC), New Delhi, India, 2021.

[Li et al., 2019]   L. Li, A.K. Abhinav, M. Collu, C. Ruzzo, F. Arena, Analysis of the coupled dynamics of an offshore floating multi-purpose platform, part a: rigid-body analysis, in: Proceedings of the 38th International Conference on Ocean, Offshore {\&} Arctic Engineering - OMAE 2019, Glasgow, UK, 2019.

[Mas-Soler and Simos, 2020]   J. Mas-Soler, A.N. Simos, A Bayesian wave inference method accounting for nonlinearity related inaccuracies in motion RAOs, Appl. Ocean Res. 99 (2020) 102125, https://doi.org/10.1016/j.apor.2020.102125.

[Melikoglu, 2018]   M. Melikoglu, Current status and future of ocean energy sources: a global review, Ocean Eng. 148 (2018) 563–573, https://doi.org/10.1016/j.oceaneng.2017.11.045.

[Muggiasca et al., 2021]   S. Muggiasca, F. Taruffi, A. Fontanella, S. Di Carlo, H. Giberti, A. Facchinetti, M. Belloli, Design of an aeroelastic physical model of the DTU 10MW wind turbine for a floating offshore multipurpose platform prototype, Ocean Eng. 239 (2021) 109837, https://doi.org/10.1016/j.oceaneng.2021.109837.

[Nassar et al., 2020]   W.M. Nassar, O. Anaya-Lara, K.H. Ahmed, D. Campos-Gaona, M. Elgenedy, Assessment of multi-use offshore platforms: structure classification and design challenges, Sustainability 12 (2020) 1860, https://doi.org/10.3390/su12051860.

[O'Donnell, Murphy and Pakrashi, 2020]   D. O'Donnell, J. Murphy, V. Pakrashi, Comparison of response amplitude operator curve generation methods for scaled floating renewable energy platforms in ocean wave Basin, ASME Lett. Dyn. Syst. Control 1 (2020), https://doi.org/10.1115/1.4049169.

[Ohanaetal2022]   Ohana, J., Horel, B., Merrien, A., Arnal, V., Bonnefoy, F., Brizzi, G., Bouscasse, B., 2022. Wave tank testing of a multi-purpose platform with aquaculture, wind turbine and wave energy converters (dataset). 10.17882/88376

[Orphin, Nader and Penesis, 2022]   J. Orphin, J.-R. Nader, I. Penesis, Size matters: scale effects of an OWC wave energy converter, Renew. Energy 185 (2022) 111–122, https://doi.org/10.1016/j.renene.2021.11.121.

[Petromichelakis and Kougioumtzoglou, 2021]   I. Petromichelakis, I.A. Kougioumtzoglou, A computational algebraic geometry technique for determining nonlinear normal modes of structural systems, Int. J. Non. Linear. Mech. 135 (2021) 103757, https://doi.org/10.1016/j.ijnonlinmec.2021.103757.

[Qiu et al., 2014]   W. Qiu, J. Sales Junior, D. Lee, H. Lie, V. Magarovskii, T. Mikami, J.-M. Rousset, S. Sphaier, L. Tao, X. Wang, Uncertainties related to predictions of loads and responses for ocean and offshore structures, Ocean Eng. 86 (2014) 58–67, https://doi.org/10.1016/j.oceaneng.2014.02.031.

[Ruzzo et al., 2018]   C. Ruzzo, V. Fiamma, M. Collu, G. Failla, V. Nava, F. Arena, On intermediate-scale open-sea experiments on floating offshore structures: Feasibility and application on a spar support for offshore wind turbines, Mar. Struct. 61 (2018) 220–237, https://doi.org/10.1016/j.marstruc.2018.06.002.

[Ruzzo et al., 2022]   C. Ruzzo, V. Fiamma, A. Scialò, F. Arena, A. Santoro, S. Muggiasca, F. Taruffi, S. Di Carlo, I. Larrea, P. Corvaglia, A. Zuccarino, F. Lagasco, Field experimental campaign on a multi-

purpose floating structure: set-up description, in: Proceedings of the 5th International Conference on Renewable Energies Offshore (RENEW2022), CRC Press /Balkema, 2022, p. 118 p. Paper n.

[Ruzzo et al., 2021]   C. Ruzzo, S. Muggiasca, G. Malara, F. Taruffi, M. Belloli, M. Collu, L. Li, G. Brizzi, F. Arena, Scaling strategies for multi-purpose floating structures physical modeling: state of art and new perspectives, Appl. Ocean Res. 108 (2021) 102487, https://doi.org/10.1016/j.apor.2020.102487.

[Ruzzo et al., 2020]   C. Ruzzo, A. Romolo, G. Malara, F. Arena, F. Taruffi, S. Muggiasca, M. Belloli, B. Bouscasse, J. Ohana, A. Santoro, K. Aubriere, G. Brizzi, M. Collu, P. Corvaglia, F. Lagasco, On the arrangement of two experimental activities on a novel multi-purpose floating structure concept, in: Proceedings of the 4th International Conference on Renewable Energies Offshore (RENEW2020), Lisbon, Portugal, 2020 October 12-15.

[SarpkayaandIsaacson1981]   Sarpkaya, T., Isaacson, M., 1981. Mechanics of wave forces on offshore structures. 10.1016/0261-7277(82)90028-6

[Wen et al., 2020]   B. Wen, X. Tian, X. Dong, Z. Li, Z. Peng, W. Zhang, K. Wei, Design approaches of performance-scaled rotor for wave basin model tests of floating wind turbines, Renew. Energy 148 (2020) 573–584, https://doi.org/10.1016/j.renene.2019.10.147.

[BGFprojectwebsite]   The Blue Growth Farm project website. Accessed: May 2022 - http://www.thebluegrowthfarm.eu/ - 2022